COMMUNICATION

Supporting Information

Inhibited-Nanophase-Separation Modulated Polymerization for Recoverable Ultrahigh-Strain Biobased Shape Memory Polymers

Guochao Fan, Huige Yang, Yunhe Diao, Shilin Tian, Tengzhou Yang, Qingqing Sun, Chuan Liu, Xuying Liu, Yaming Wang, Chunguang Shao, Chuntai Liu, Hongzhi Liu, Wentao Liu, Miaoming Huang, Hao Liu, Jinzhou Chen, Yanlin Song
E-mail: liuxy@zzu.edu.cn

COMMUNICATION

Experimental section

Soxhlet Extraction Experiment: The rectangular polymer film with the size of 30 mm × 30 mm × 1 mm is immersed into chloroform to remove short chains and unreacted monomers at 80℃ for 30 h. Then, the extracted film is syringed by deionized water for 3 min. After drying at 80℃ for 3 h, the gel fraction can be calculated according to the following Equation (1):

$$Gel\ Fraction(\%) = \frac{W_{before} - W_{after}}{W_{before}} \times 100\%$$

Where Wbefore and Wafter are the weight of the initial PBDC polymer and dried insoluble part of the sample, respectively.

Thermal Analysis: The phase transition temperature of PBDC polymers was studied by using DSC204 (NET2SCH, Germany). All samples are firstly heated at 150 ℃ for 3 min to remove thermal history, and then rapidly cooled by -50 ℃. Finally, the heat-cooled sample are heated by 150 ℃ at the rate of 10 ℃/min. While thermal stability of PBDC polymers is measured by thermogravimetric analysis (TGA) using TG209(Germany). All measurements are performed under nitrogen gas condition from 25 ℃ to 600 ℃ at a heating rate of 10℃/min.

The water contact angle measurement: The water contact angle was measured with a JC 2000A contact angle measuring instrument by using 4-5 μL water droplets. The average contact angle values were obtained by measuring the same sample in five different positions. The detailed process is as follows: Firstly, putting the water droplet on the matrix to measure and record the WCA before stretching the matrix, and then remove water drops. Secondly, with the strain of 5%, 15%, 40%, 50%, 70%, 100%, 120%, the different positions of the matrix were fixed. Then, the WCA of the matrix was measured and recorded by the same way. Finally, the WCA of the same status was measured by the same way during the release process of the strain.

Other characterizations: The chemical structures of PBDC polymers are characterized by Fourier transform infrared spectroscopy (bruker tensor II, Germany) in a range from 500 to 4000 cm^{-1} via a reflectivity mode at room temperature. The typical stress-strain curve is obtained by UTM2502 (Shenzhen), and the related sample size is 40×15×1 mm. The surface morphologies of the prepared 7%-PBDC polymer are characterized by Zeiss/Auriga FIB SEM (Germany). The water contact angle is measured by JC2000A (Zhong Chen Digital Equipment Technology Co., Ltd, China).

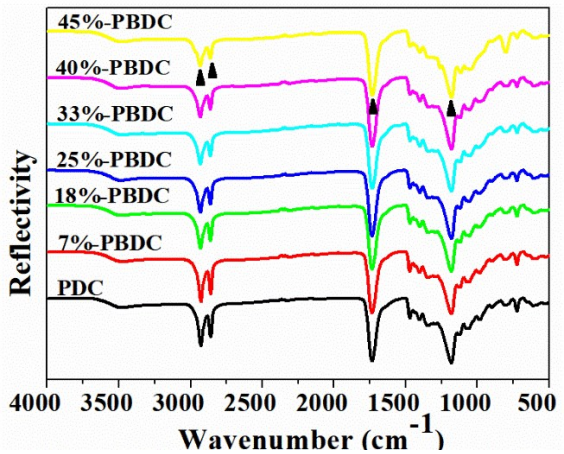

Figure S1. FT-IR reflection spectra of all PBDC polymers.

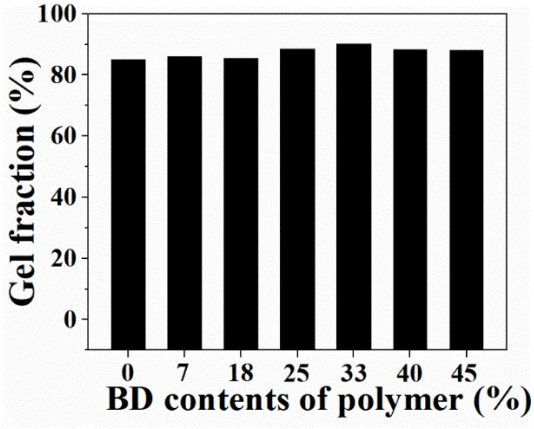

Figure S2. The Gel fraction of all PBDC.

Table S1. The phase transition temperature, the decomposition temperature as well as the mechanical property of PBDC polymers.

S. No.	T_{trans} (℃)	T_{start} (℃)	T_{max} (℃)	T_{end} (℃)	Residual Mass (%)	Strain (%)
PDC	7.0	273.0	364.4	456.2	4.8	399.0
7%-PBDC	4.2	282.0	368.8	458.8	3.6	764.0
18%-PBDC	-1.0	272.0	365.6	469.1	5.2	129.0
25%-PBDC	-17.7	272.3	362.5	458.2	4.6	78.0
33%-PBDC	-14.8	287.8	370.5	469.3	4.2	77.5
40%-PBDC	-11.5	279.3	365.0	443.2	3.9	76.7
45%-PBDC	-12.3	265.8	360.1	440.5	5.8	76.5

Notes: T_{trans} represents the phase translation temperature; T_{start}, T_{max} and T_{end} stand for the different decomposition temperatures.

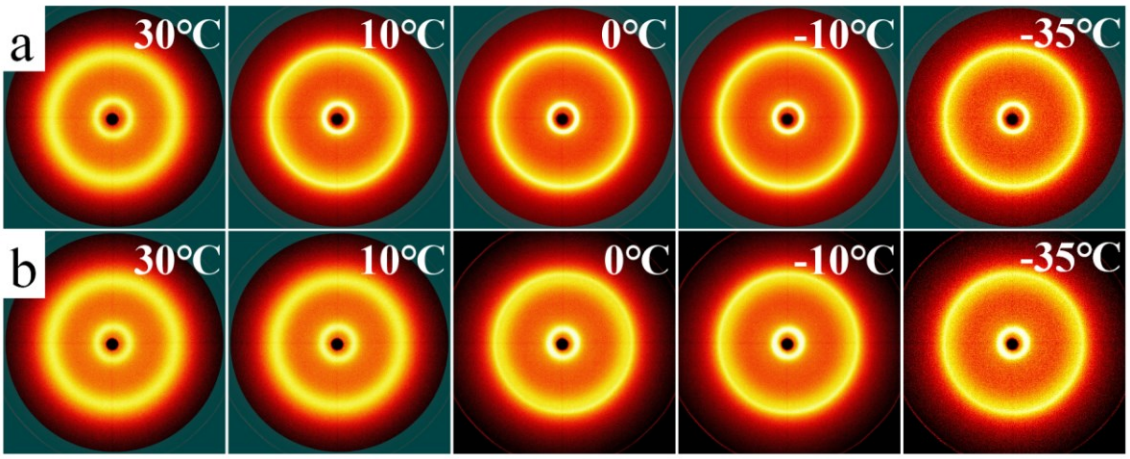

Figure S3. 2D-WAXD patterns of (a) PDC and (b) 18%-PBDC polymers during the cooling process.

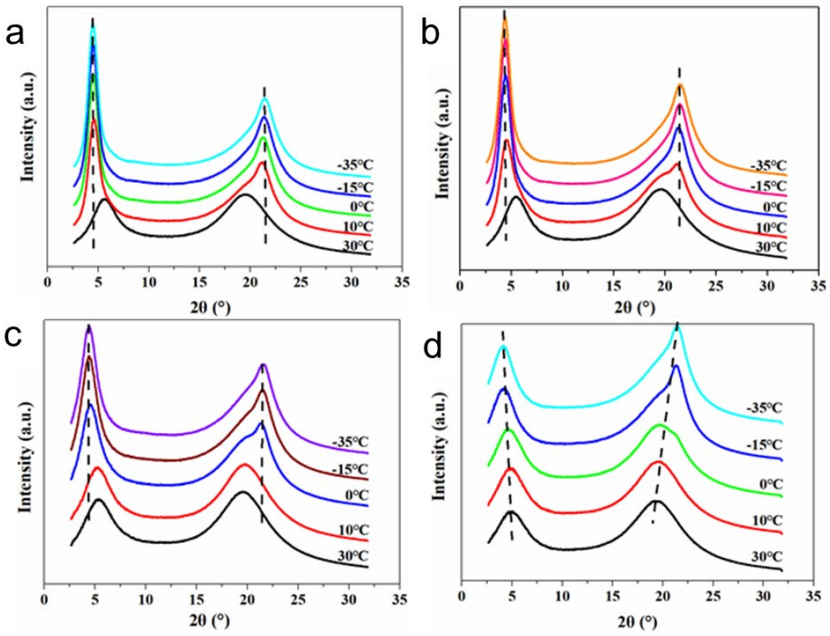

Figure S4. XRD patterns of PDC (a), 7%-PBDC(b), 18%-PBDC (c) and 33%-PBDC polymers during the cooling process.

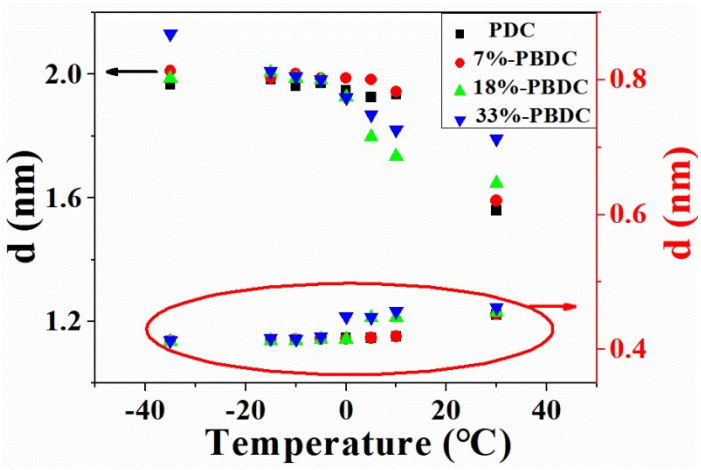

Figure S5. Temperature-dependent d-spacing of PBDC polymers. The related d-spacing can be calculated by Bragg Equation (2)[S1]:

$$2d \sin\theta = n\lambda \quad (2)$$

Where d is the spacing between diffracting planes, ϑ is the incident angle, n is any integer, and λ is the wavelength of the beam.

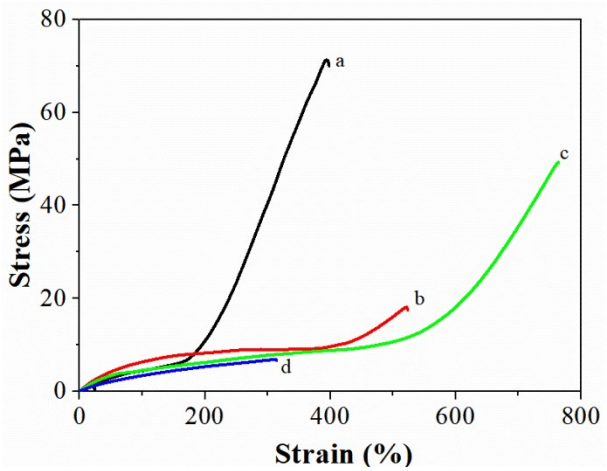

Figure S6. Tensile stress-strain curves of PDC (a), 5%-PBDC (b), 7%-PBDC (c), 10%-PBDC (d) polymers. To check whether 7%-PBDC polymer has ultrahigh strain, 5%-PBDC and 10%-PBDC polymers are prepared.

Table S2. Material characteristic properties and preparation of bio-shape memory polymer in recent years.

Year	Material type	Preparation	Strain at break	R_f	R_r	Ref
2015	epoxy-based SMP	solution	490%	95%	98%	S2
2016	PLLA-baded SMP	--	600%	99%	94%	S3
2016	POMaC	assembly and photo-crosslinking	150%	--	--	S4
2017	PU- PCL-PLLA	synthesized with some modification based on the literature	384%	74.5 ± 5%	87.2 ± 3.8%	S5
2017	polycaprolactone	ring-opening polymerizationreaction	400%			S6
2018	vitrimer-based SMP	UV-curing	43%	100%	99%	S7
2019	graded metamaterials	3D printing	over 75%	--	--	S8
2019	liquid crystalline SMP	--	500%	--	--	S9
2019	semi-IPN elastomer	--	600%	--	--	S9
2020	(TPI)	--	480%	--	100%	S10
--	PBDC SMP	Inhibited-Nanophase-Separation Modulated Polymerization	770%	99%	98%	This work

Note: PLLA: Poly(L-lactic acid); POMaC: poly(octamethylene maleate (anhydride) citrate); PU: Polyurethane; PCL: polycaprolactone; TPI: trans-1,4-polyisoprene

Mechanism of shape memory: To further understand how to reversibly transform from their permanent shape to a temporary shape upon thermal stimulation, mechanisms of shape memory are presented in Figure S1. Briefly, the polymer chains form a hard domain (rich phase) and a reversible phase (poor phase) in cross-linked manner. When the temperature rises above the phase transition temperature (i), the microscopic brownian movement of the reversible phase molecular chain is intensified, while the hard phase is still in a solidified state. At this time, the PBDC polymers are deformed by a certain external force, and the external force is maintained to cool (ii). The reversible phase solidification results in a temporary shape. When the temperature rises again (iii), the reversible phase softens, while the hard phase remains solidified, and the reversible phase molecular chain movement is revitalized. Thus the thermodynamic equilibrium state is gradually achieved under the action of the restoration stress of the hard phase. Finally, the permanent shape is presented.

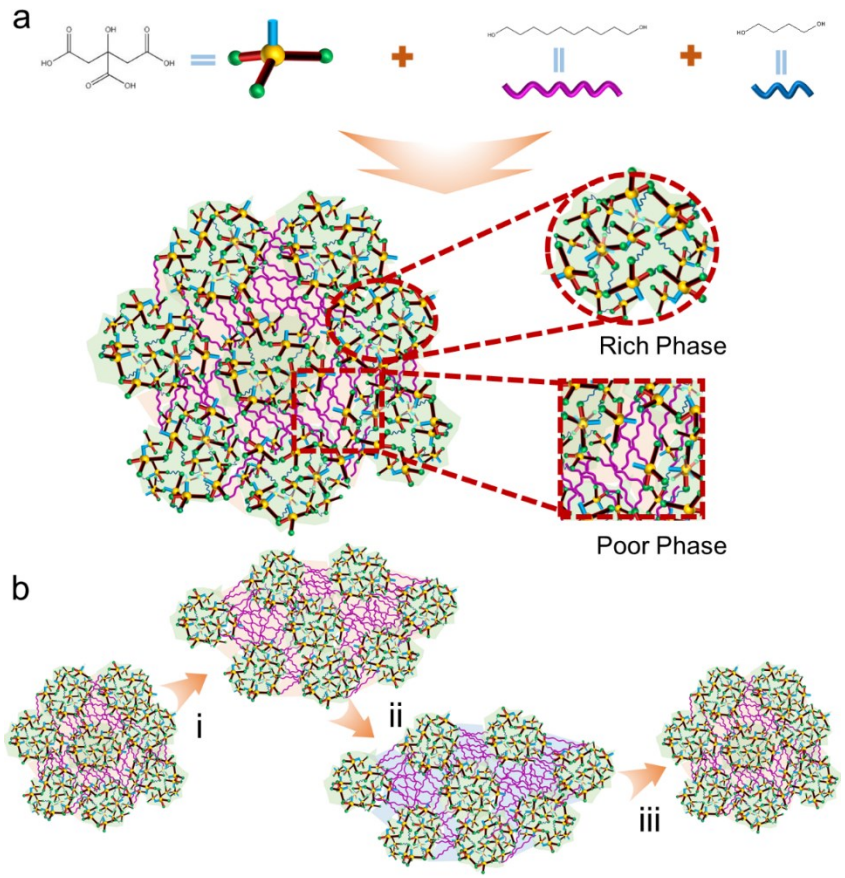

Figure S7. Schematic illustration of PBDC polymers. a) Chemical structures and the synthetic mechanism for preparing PBDC polymers. b) The shape memory mechanism of PBDC polymer to thermal stimulation.

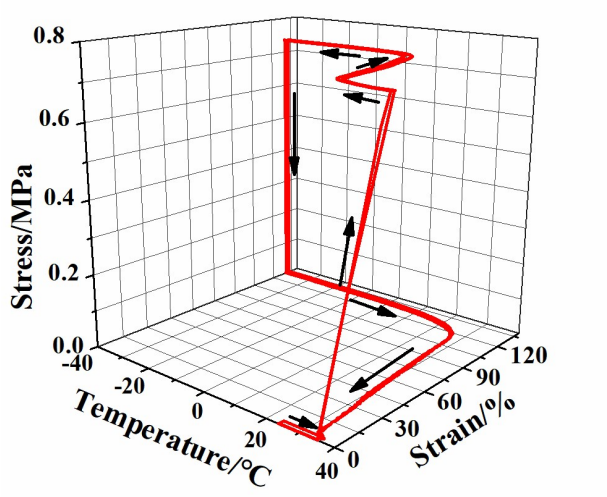

Figure S8. Three-dimensional stress-strain-temperature curve for the PDC polymer. To discuss about the stability of shape memory, shape memory processes are tested in two cycles. After the first cycle the temperature is kept constant for 5 min to allow the polymer fully recovery. As exhibited, the strain of the sample hardly changes after two cycles, which indicates PDC polymer has a excellent shape memory stability.

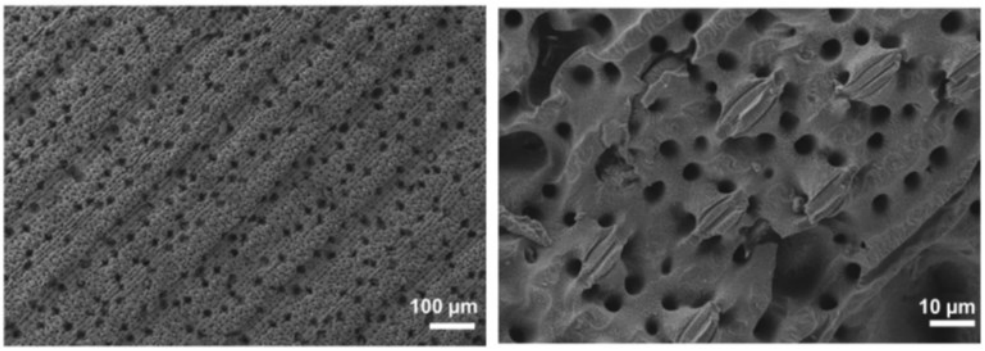

Figure S9. SEM images of the PDMS soft template. The morphology of soft template demonstrates the complementarity with morphology of the bamboo leaves.

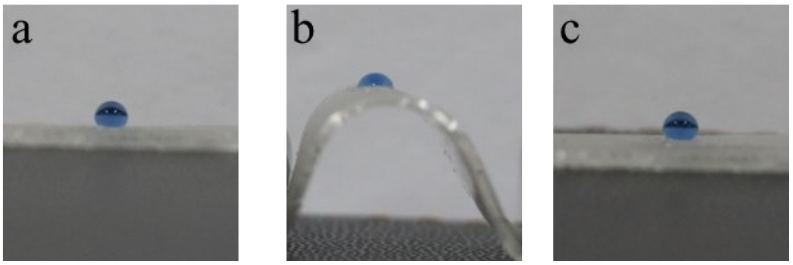

Figure S10. Tunnable wettability on the surface of 7%-TS-PBDC polymer during bending process. a) initial state; b) bending state; c) recovered state.

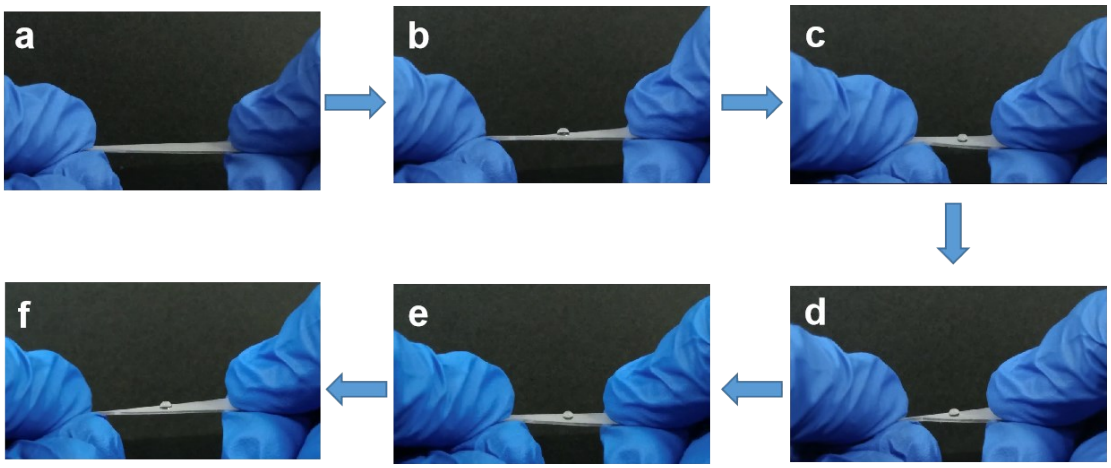

Figure S11. （a-c) and (d-f) is the changes of WCA during the stretching and recovering processes, respectively.

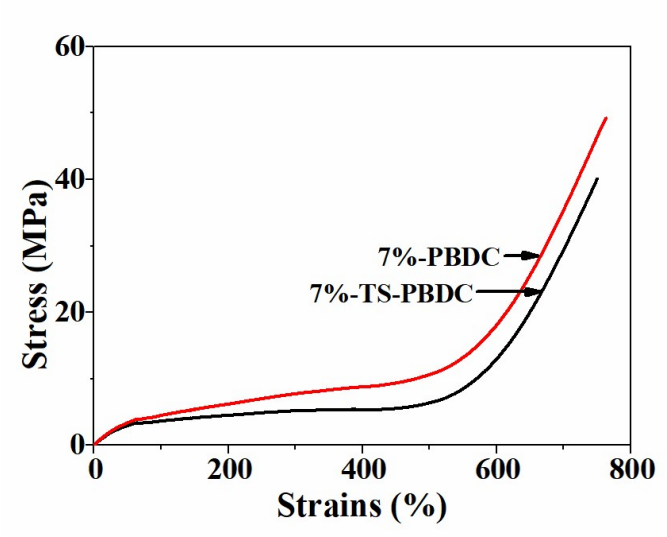

Figure S12. Stress-strains curves of 7%-PBDC and 7%-TS-PBDC polymer.

References:

S1 A. P. M. Araúj`o, P. Agrawal, S. N. Cavalcanti, A. M. Alves, G. F. Brito, *Macromolecular Symposia* 2014, 343, 59-64.
S2 S.S. Pulla, M. Souri, H.E. Karaca, Y.C. Lu, *Journal of Applied Polymer Science* 2015, 132, 41861.
S3 M. Balk, M. Behl, C. Wischke, J. Zotzmann, A. Lendlein, *Adv Drug Deliv Rev*, 2016, 107, 136-152.
S4 B. Zhang, M. Montgomery, M. D. Chamberlain, S. Ogawa, A. Korolj, A. Pahnke, L. A. Wells, S. Masse, J. Kim, L. Reis, A. Momen, S. S. Nunes, A. R. Wheeler, K. Nanthakumar, G. Keller, M. V. Sefton, M. Radisic, *Nat. Mater* 2016, 15, 669.
S5 Y. C. Chien, W. T. Chuang, U. S. Jeng, S. H. Hsu, *ACS Appl. Mater. Interfaces* 2017, 9, 5419.
S6 M. Montgomery, S. Ahadian, L. D. Huyer, M. Lo Rito, R. A. Civitarese, R. D. Vanderlaan, J. Wu, L. A. Reis, A. Momen, S. Akbari, A. Pahnke, R. K. Li, C. A. Caldarone, M. Radisic, *Nat. Mater*, 2017, 16, 1038.
S7 A. Li, J. Fan, G. Li, *Journal of Materials Chemistry A*, 2018, 6, 11479-11487.
S8 X. Kuang, J. Wu, K. Chen, Z. Zhao, Z. Ding, F. Hu, H.J. Qi, *Science Advances*, 2019, 5, 5790.
S9 A. Kirillova, L. Ionov, *J Mater Chem B*, 2019, 7, 1597-1624.
S10 J. Liu, B. Min, Z. Wang, J. Teng, X. Sun, S. Li, S. Li, *Nanoscale* 2020,12,3205-3219.

Please do not adjust margins